Analyst

Enzyme kinetics in confined geometries at a single enzyme level

Journal:	*Analyst*
Manuscript ID	AN-ART-11-2021-002024.R2
Article Type:	Paper
Date Submitted by the Author:	07-Feb-2022
Complete List of Authors:	Murahara, Hisashi; Nagoya University Kaji, Noritada; Kyushu University Tokeshi, Manabu; Hokkaido University, Division of Applied Chemistry Baba, Yoshinobu; Nagoya University, ImPACT Research Center for Advanced Nanobiodevices

ARTICLE

Enzyme kinetics in confined geometries at a single enzyme level

Hisashi Murahara,[a] Noritada Kaji, *[b,c] Manabu Tokeshi [c,d] and Yoshinobu Baba [a,c,e,f]

Received 00th January 20xx,
Accepted 00th January 20xx

DOI: 10.1039/x0xx00000x

The effects of increased confinement on the catalytic rates of individual enzyme molecules were studied at a single molecule level using femtolitre chambers and molecular crowders. According to the increase of confinement, from micro to nanometer cubic space in the chambers, the hydrolysis rate of *β*-galactosidase (*β*-gal) was decreased to one-tenth of the rate in bulk. When molecular crowders suppressed the diffusion rates that reduces the collision chance of an enzyme and a substrate, the hydrolysis rate was also decreased, as well as in the femtolitre chambers. However, their kinetic trend was different especially from the viewpoint of the diffusion rates in diffusion-limited space. These data suggested that cell or organelle-scale confined environments might affect kinetics of biochemical reactions and emphasized the importance of understanding enzyme kinetics *in vivo* environment.

Introduction

More than 100 years have passed since Michaelis and Menten published their first original paper predicting the Michaelis-Menten equation which quantitatively described the rate of an enzyme-catalyzed reaction.[1] For a long period of time, enzyme kinetics have been studied by ensemble of the enzymatic reactions. Thanks to recent development of micro- and nanofabrication technologies in semiconductor industry, a single enzyme kinetics have been explored by Noji *et al*. using femtolitre-size chambers which enable to capture a single enzyme in a small reaction tube.[2] At around the same time, another approach has been proposed by Walt *et al.* using a 1 mm femtoliter chambers array located on the end of an optical fiber bundle and abled to capture and readout the signals from single enzyme molecules.[3, 4] Noji *et al.* applied the femtolitre chamber platform for various enzyme-based assay studies, for example, membrane transport activity assay such as *α*-hemolysin and F_oF_1-ATP synthase coupled with an arrayed lipid bilayer chambers,[5] multiple single-molecule bioassays in parallel using alkaline phosphatase or *α*-hemolysin micro-reactor (4 μm in diameter and 0.5 μm in height) arrays with a concentration gradient of target molecules,[6] and single enzyme activity-based assays for various phosphoric ester-hydrolyzing enzymes in blood samples.[7] In their femtolitre chamber platform, it was reported that smaller and shallower reaction chambers about 200 aL (3.0 μm in diameter and 30 nm in height) enhanced the sensitivity, throughput, and accuracy of massively parallel single-molecule assay of membrane transporter activity.[8] The characteristics of micro-scale analysis system such as increasing sensitivity and accelerate reaction speeds were further applied for highly efficient protein synthesis[9] and antibody-free digital influenza virus counting[10, 11] as a point-of-care device. The chamber platform is useful not only for biochemical assay but also understanding biochemical reactions inside a cell or an organelle. Walt *et al.* scrutinized enzyme kinetics using stochastic inhibitors[12] and the mutants.[13] Although the confinement in the chamber platform accelerate diffusion-limited reactions such as antigen-antibody reaction and protein synthesis *in vitro* experiments, we do not know whether the further reduction of reaction space from micro to nanometer scale can simply extrapolate from a single enzyme kinetics observed in bulk or micrometer scale chambers or not.

Another approach to mimic confined intracellular environments is a method using molecular crowders like polyethylene glycol (PEG) which alters molecular behaviors by changing diffusion coefficient, water activity, and excluded volume effect. In prokaryotes and eukaryotes, the cell's interior is crowded by high concentration of macromolecules giving from 200 to 400 mg/mL, which reduced the available volume of solvent for the macromolecules.[14] Such a molecular crowding environment might be equivalent to being confined in a very small space like the above femtolitre chamber platform from a viewpoint of diffusion-limited environment and may affect the enzyme kinetics. The molecular environment has been quantitatively discussed from thermodynamics and kinetics using nucleic acids[15] and proteins including enzymes[16] due to the dual nature of molecular crowders against target molecules, exclusion volume effect and interactions via water molecules.[17] In microtube experiments containing high concentration of the molecular crowders, it is quite difficult to isolate the

[a] *Department of Biomolecular Engineering, Graduate School of Engineering, Nagoya University, Furo-cho, Chikusa-ku, Nagoya 464-8603, Japan*
[b] *Department of Applied Chemistry, Graduate School of Engineering, Kyushu University, 744 Motooka, Nishi-ku, Fukuoka 819-0395, Japan*
[c] *Institute of Nano-Life-Systems, Institutes of Innovation for Future Society, Nagoya University, Furo-cho, Chikusa-ku, Nagoya 464-8603, Japan*
[d] *Division of Applied Chemistry, Faculty of Engineering, Hokkaido University, Kita-13, Nishi-8, Kita-Ku, Sapporo 060-8628, Japan*
[e] *Institute of Quantum Life Science, National Institutes for Quantum and Radiological Science and Technology, Chiba, 263-8555, Japan*
[f] *School of Pharmacy, College of Pharmacy, Kaohsiung Medical University, 100, Shih-Chuan 1st Rd., Kaohsiung, 807, Taiwan, R.O.C.*

†Electronic Supplementary Information (ESI) available: [details of any supplementary information available should be included here]. See DOI: 10.1039/x0xx00000x

thermodynamics and kinetics factors affecting the enzymatic reaction. The chamber platform might be able to eliminate the thermodynamic factors and focus on a "pure" single enzyme kinetics. So, in this study, we investigated how the size of reaction space which directly links to the diffusible space in the chamber platform affect a single enzyme kinetics toward understanding of enzyme kinetics in intracellular environments.

A hydrolysis enzyme, *β*-gal, was adopted for this study because it widely used for biochemical assay and the kinetic parameters both in bulk and chamber platform are available. In this study, Fluorescein di-*β*-D-galactopyranoside (FDG) was used as a substrate of *β*-gal and the product, Fluorescein, was produced by the hydrolysis reaction. Although the hydrolysis reaction consists of two steps, the hydrolysis rate of FDG to Fluorescein mono-*β*-D-galactopyranoside (FMG) is significantly slower than of FMG to Fluorescein from the previous reports.[18, 19] Therefore, the rate-determining step is the first step, from FDG to FMG, and the all produced FMG can be fully hydrolyzed to Fluorescein. In this study, observed hydrolysis rate was calculated as considered a single step hydrolysis which essentially corresponds to sum of the two steps. The kinetic parameters, Michaelis-Menten constant K_m and hydrolysis rate k_{cat}, were reported by several groupsand concluded that all produced FMG is fully hydrolyzed to fluorescein.[19,20] In the femtolitre chamber system, Noji *et al.* observed the k_{cat} as 20 s^{-1}, which is comparable to the calculated value from the above Huang's value, 17.1 s^{-1}. Adsorbed *β*-gal onto the methylated silica surfaces showed decrease in k_{cat} by a factor of 10 and increase in K_m by a factor of 4.5.[21] Medintz *et al.* demonstrated the phenomenon of enzyme catalytic enhancement when *β*-gal immobilized on a quantum dot (QD) surface.[22, 23] Although the conjugation of QD resulted in a significant increase in the k_{cat}, the corresponding K_m values became worse, *i.e.*, lower affinity than the free enzyme. Interestingly, the activity of *β*-gal displayed on QD was enhanced about 3 to 4 times despite *β*-gal is considered as a typical diffusion-limited enzyme under standard solution-based conditions. Comprehensive understanding of these enzyme kinetics in different environments (e.g. diffusion-limited space by physical confinement, excluded volume effect, or immobilization on solid surface) is still missing and requires a step-by-step experimental system for mimicking intracellular environments.

Experimental

Enzyme kinetic assays in bulk

Fluorescein Di-β-D-galactopyranoside (FDG), β-D-Galactosidase (β-gal), Fluorescein, 2-mercaptoethanol, Ethylene Glycol (EG) and Polyethylene Glycol 8000 (PEG8000) and 20000 (PEG20000) were obtained from FUJIFILM Wako Pure Chemical Corporation (Osaka, Japan). Phosphate buffer (PB, pH=7.4), Phosphatidylcholine (PC), Ethylene Glycol (EG) and Bovine Serum Albumins (BSA) were obtained from Sigma-Aldrich Japan (Tokyo, Japan). To quantitatively analyze the effects of molecular crowding on the enzyme kinetic assay, EG, PEG8000, PEG20000, and BSA were into the assay solution as molecular crowding reagents in the concentration range of 2.5~20(w/v)%. Fluorescence measurements in a 1 cm cuvette were done using a spectrofluorometer FP-6500 (Jasco Corporation, Tokyo, Japan). Viscosity of PEG solution was measured by a portable viscometer (Viscolite 700, Hydramotion Ltd., England). All the measurements were conducted under controlled temperature at 30°C.

Device fabrication

Polydimethylsiloxane (PDMS)-based microfluidic devices were fabricated using standard soft lithography methods.[24] The master mold for the micro- and nano-chamber pattern was fabricated on a silicon substrate by electron beam (EB) lithography and Bosch etching. The fabrication process is illustrated in Figure S1. Thin (~50 nm) Cr film was sputtered on the silicon substrate. Thick (~200 nm) posi-EB resist (ZEP-520, Zeon Corp.) was spin-coated and the pillar pattern was delineated by EB lithography. After the development of the EB resist, the Cr layer was etched by Cr etchant along the pattern of the EB resist. The pillar patterns were dry-etched employing Bosch-type deep reactive ion etching (DRIE) process. Acetone and Cr etchant removed the EB resist and Cr layer on the silicon substrate, respectively. The fabricated master mold was silanized in a desiccator, which was filled with trichloro(1H,1H,2H,2H-perfluorooctyl)silane (Sigma-Aldrich Co. LLC., Tokyo, Japan) vapor prior to the addition of a mixture of a curing agent and PDMS prepolymer (SYLGARD 184 Silicone Elastomer Kit, Dow Corning Toray Co., Ltd., Tokyo, Japan) in a 1:10 weight ratio. The prepolymer mixture was degassed in a vacuum desiccator for 2 h and then cured for 2 h at 80 °C. The PDMS replica was peeled from the master and the surface of the PDMS replica was treated using soft plasma etching equipment (SEDE-PFA, Meiwafosis Co., Ltd., Tokyo, Japan) for 90 s at 5 mA just before use. In this research, three different sizes of micro- and nanometer-scale chambers were fabricated, 61 fL(φ:4.0 μm×H:5.1 μm), 61 fL(φ:4.0 μm×H:5.1 μm), 61 fL(φ:4.0 μm×H:5.1 μm).

Single enzyme kinetic assays in microchambers

The assay flow, the configuration of the microchamber array, and the reaction scheme are shown in Figures 1 (A)-(C), respectively. A surface of a cover glass was spin-coated by uncured PDMS at 3000 rpm for 60 s, and then, the PDMS was cured for several hours in room temperature. The mixed solution of β-gal and FDG was dropped onto the PDMS-coated cover glass and clamped by the microchamber device. Spontaneous adhesion of PDMS achieved perfect sealing of the solution in the microchamber. The enclosed microchamber device was put on the stage of total internal reflection fluorescence microscope (TIRFM, IX71, Olympus, Tokyo, Japan) equipped with argon-ion laser (488 nm) and bright field images were captured quickly (typically less than 10 s) to recognize the location and the contour of the individual chambers at first, and then, the fluorescence in the microchambers were observed through high magnification objective lenses (UAPON150×OTIRF, UPLAPO100×OHR, UPLAPO60×OHR) under evanescent wave illumination. The all observation experiment was performed at 30°C using stage top incubator (TOKAI HIT Co., Ltd., Fujinomiya, Japan). The fluorescent images were captured by an image intensifier unit (C8600, Hamamatsu Photonics, Hamamatsu, Japan) coupled to an EB-CCD camera (C7190, Hamamatsu Photonics) and analyzed the fluorescence intensities at originally recognized location of the individual chambers by an image analysis software (Aquacosmos, Hamamatsu Photonics)

In order to suppress non-specific adsorption onto the PDMS surface, phosphatidylcholine (Merk KGaA, Darmstadt, Germany) were used to form supported lipid bilayers (SLBs) on the surface. Phosphatidylcholine was dissolved in chloroform at 10(w/v)% and dried out under nitrogen gas flow for half a day. The deposited film consisting of stacked phospholipid bilayer was subsequently hydrated in 100 mM phosphate buffer under ultrasound treatment and size-reduced multi-lamellar vesicles were obtained. The prepared liposome solution was diluted to a concentration of 0.25 ng/mL and used for the PDMS surface coating.[25, 26]

Enzyme kinetic assays under molecular crowding conditions

The basic assay solution was prepared by mixing β-gal and FDG (50, 100, 200 μM) in 100 mM phosphate buffer (pH=7.5) containing 1 mM MgCl2 and 0.2(v/v)% 2-mercaptoethanol. To reproduce the intracellular molecular crowding environment, molecular crowding agents including ethylene glycol (EG) (FUJIFILM Wako Pure Chemical Corporation, Osaka, Japan), bovine serum albumin (BSA) (Merck KGaA, Darmstadt, Germany), PEG8,000 (PEG with an average molecular weight [Mw] of 8,000) and PEG20,000 (PEG with Mw of 20,000) (FUJIFILM Wako Pure Chemical Corporation, Osaka, Japan), were added into the assay solution in the concentration range of 2.5 wt% to 20 wt%. The fluorescence intensity was monitored by a fluorescence spectrophotometer (FP-6500, JASCO Corporation, Tokyo, Japan) at Excitation/Emission wavelength = 490 nm/520 nm at 30 °C temperature. Viscosity of the solution containing molecular crowding agents was measured by a Viscolite 700 Portable Viscometer (Hydramotion, York, UK). The all experiments under molecular crowding conditions were performed in bulk using 1.5-mL microtubes.

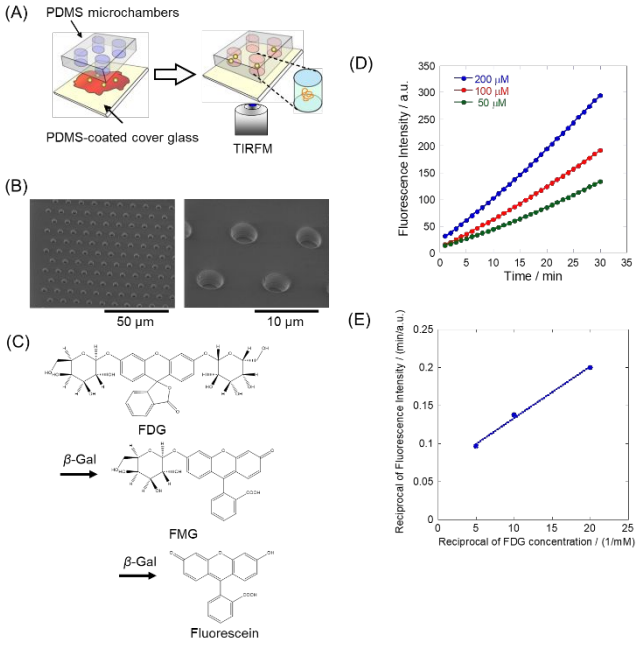

Figure 1. (A) Schematic illustration of the experiment. The PDMS-fabricated microchamber device was pushed onto the PDMS-coated cover glass containing the reaction solution. The fluorescence intensity of the enclosed reaction solution was observed by a TIRFM. (B) SEM images of the microchamber array (diameter = 4 μm (61 fL)). (C) Reaction scheme of the hydrolysis of FDG by *β*-Gal. (D) Enzyme reaction kinetics in the bulk at 30 °C. Time courses of the fluorescence intensities of the produced fluorescein at different FDG concentrations (inset of the figure. (E) Double-reciprocal plot of the hydrolysis of FDG. The regression curve was $y = 0.0068x + 0.065$, $R^2 = 0.99$.

Results and Discussion

Enzyme kinetic assays in bulk

Ensemble-averaged kinetic measurements of *β*-gal were performed at microliter to milliliter scale using 1-cm square cuvette as a control experiment for the following single enzyme kinetic studies. To estimate Micahelis-Menten constant K_M and hydrolysis rate k_{cat}, the time course of the fluorescence intensity produced by the *β*-gal reaction was measured at various concentrations of FDG as shown in Figure 1(D). As the time is elapsed (>10 min), the derivative of the fluorescence intensity, dF/dt, converged to a constant value and can be assumed as a single step hydrolysis even in this two-step hydrolysis reaction, which corresponds to apparent k_{cat} at a certain FDG concentration. Because the hydrolysis rate of FDG to FMG is significantly slower than of FMG to Fluorescein, the plots are expected to be linear depending on the hydrolysis rate of FDG to FMG. However, several reports suggested sigmoidal increase of Fluorescein signal by *β*-gal and the reason is still not clear.[18,19,27] A potential explanation is that there exists transient kinetics or pre-steady states involving the stability of intermediate complex and the dissociation (or release) rate constant complex.[28,29] The complete discussion is beyond the

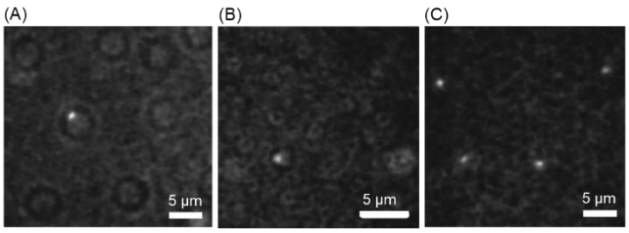

Figure 2. Liquid leakage and evaporation checks to confirm the reaction microspace that was formed by the microchamber devices. The microchambers of (A) 61 fL(*ϕ*:4 μm, H:5.1 μm), (B) 7.2 fL(*ϕ*:2.4 μm, H:1.6 μm), and (C) 510 aL(*ϕ*: 850 nm, H:900 nm)-enclosed fluorescent nanobeads (diameter = 50 nm) were observed via the TIRFM. The fluorescent images were acquired under illumination from weak transmitted light to extract the contour of the microchambers. The Brownian motion of the nanobeads proceeded for >1 h in all the microchambers, indicating that the microchamber devices behaved as completely sealed test tubes. The movies of the Brownian motion are available in the Supporting Information (SI).

scope of this paper, hence the apparent k_{cat} observed after a certain time of period was adopted as k_{cat} in this study. When FDG concentration is high enough to employ all the available *β*-gal and the reaction becomes saturated, k_{cat} can be calculated using the following equation:

$$\frac{dF}{dt} = \frac{\alpha k_{cat} E S_0}{K_M + S_0} \qquad (1)$$

where α is the constant (1234 a.u.·μM^{-1}) that represents the fluorescence emission intensity of Fluorescein (arbitrary units: a.u.) detected by the spectrofluorometer at 514 nm, E is the *β*-gal concentration, and S_0 is the initial FDG concentration. With the use of eq. (1), a double-reciprocal plot of $1/k_{cat}E$ versus $1/S_0$ yielded a linear curve as shown in Figure 1(E) and gave K_M = 86.2 μM and k_{cat} = 18.0 s^{-1}, which is consistent with earlier reports of 17.1 s^{-1} [19] and 20 s^{-1}.[2] In this paper, we focused on how diffusion-limited space in enzyme reactions affect k_{cat} under physical confinement and molecular crowding conditions.

Single enzyme kinetic assays in micro- and nanochambers

Owing to the extremely small reaction volume, water leakage or evaporation in micro- and nanochambers is a critical issue during the quantitative analysis of enzyme reaction kinetics. When the buffer solution was sealed with the chambers which were treated with soft plasma etching equipment before sealing, the boundaries of the chambers could be observed as shown in Figure S2. However, after five minutes, they became quickly invisible because of the liquid evaporation. This might be due to the well-known gas permeability of PDMS.[30, 31] To prevent the quick liquid evaporation in the chambers, pre-soaked PDMS chambers in buffer solution for several hours were adopted for the following assay experiments. To confirm the stable reaction space for a certain time, fluorescent nanoparticles of 50-nm diameter was enclosed inside the chambers and observed the motion by TIRFM. In order to prevent non-specific adsorption of the nanoparticles onto the PDMS surface, BSA was dissolved into the water containing the nanoparticles at 10 mg/ml and applied to the observation experiment. Figure 2 and Supplementary movie S1 show that Brownian motion of the nanoparticles inside the

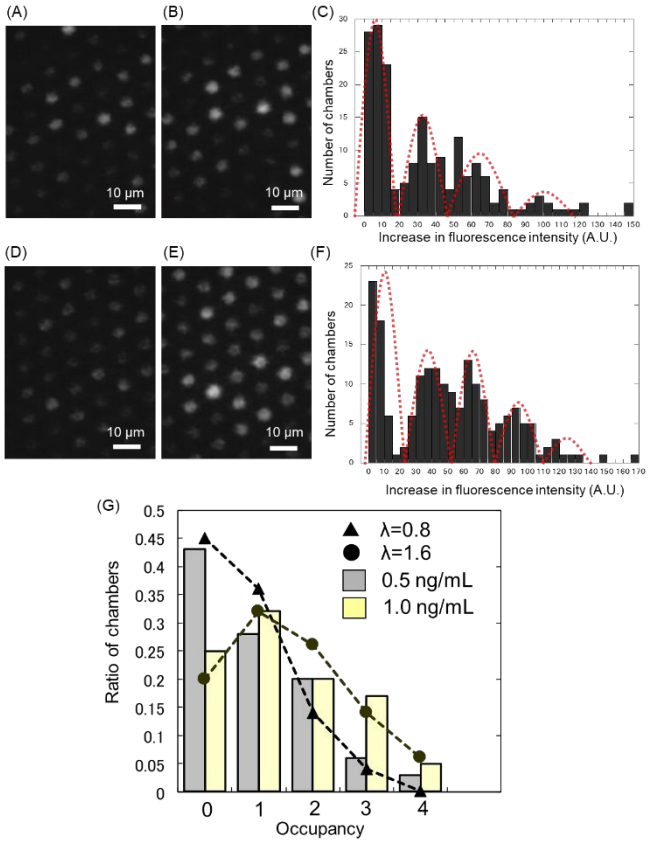

Figure 3. Single-enzyme assay in the 61-fL chambers. The fluorescent images of the microchamber array enclosing *β*-gal after times (A) 0 and (B) 2 min. (C) Histogram of the fluorescent intensity changes for 2 min (n = 187). The concentrations of *β*-Gal and FDG were 0.5 ng/mL and 200 μM, respectively. (D–F) The same experiment was performed with double concentrations of *β*-gal (1.0 ng/mL) (n = 191). The concentration of FDG was 200 μM. The four peaks in (C) and five peaks in (F) were attributable to the occupancies of 0, 1, 2, 3, and 4 enzymes per a microchamber. The red-dotted lines are guides to the eyes on the assumption of a normal gaussian distribution. (G) Occupancy distribution of the microchambers under the two conditions (0.5 and 1.0 ng/mL *β*-gal in gray and yellow colors, respectively. The bars show the ratio of the microchambers with an occupancy of N enzymes (N = 0, 1, 2, 3, 4). The triangles and circles indicate the probability of the ratio of the microchambers that were captured N enzymes at λ = 0.8 and 1.6, respectively, assuming it was a Poisson distribution. The detail explanation is described in the main text. All the fluorescent images were captured under the illumination of a 17.9 μW excitation laser.

microchambers and this motion was observed over 1 hour. The pre-soaked PDMS microchambers were effective to make stable reaction chambers suppressing water leakage and evaporation.

Firstly the 61-fL microchambers were used for a single *β*-gal kinetic assay. The assay solution containing 200 μM of FDG and 0.5 ng/ml or 1.0 ng/ml of *β*-gal in phosphate buffer was enclosed inside the microchambers and the fluorescent images were captured at time 0 and 2 minutes. To prevent photobleaching, a shutter for the excitation light was closed during the time interval. The fluorescence bleeding from adjacent chambers were not observed throughout the whole experiments. As shown in Figure 3, the number of microchambers which showed clear changes of fluorescence intensity was increased by doubling the *β*-gal concentration. From these fluorescent images in Figure 3(A, B, D, E), histograms of the increase of fluorescent intensity were made

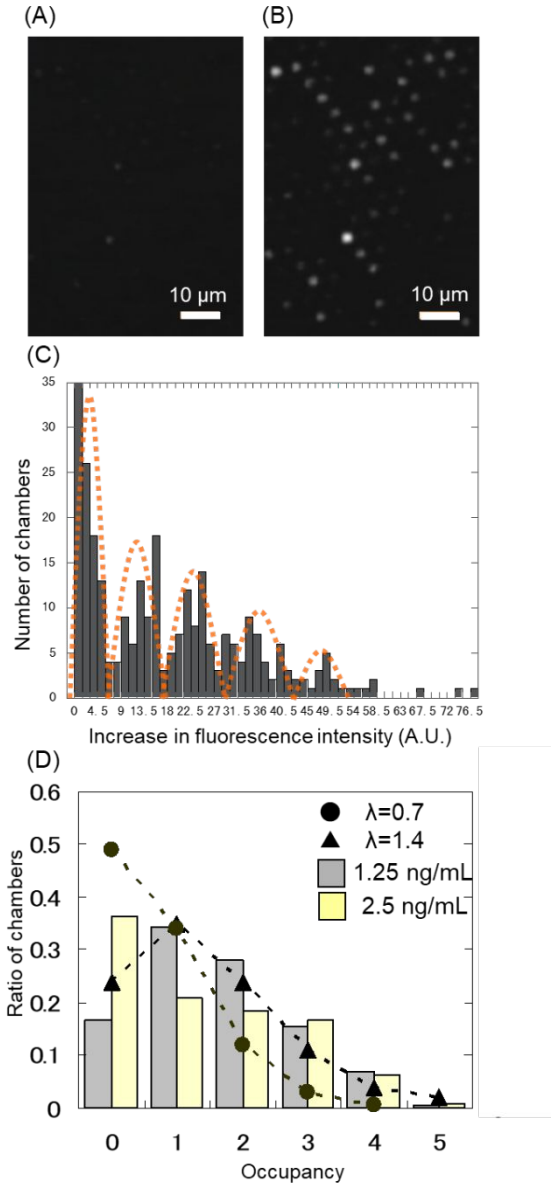

Figure 4. Single-enzyme assay in the 7.2-fL chambers. Fluorescent images of the microchamber array-enclosed *β*-gal at times (A) 0 and (B) 1 min. (C) Histogram of the fluorescent intensity changes for 2 min (n = 283). The concentration of *β*-gal and FDG were 1.25 ng/mL and 200 μM, respectively. The five peaks in (C) are attributable to the occupancies of 0, 1, 2, 3, and 4 enzymes per chamber. The red-dotted lines are guides to the eyes on the assumption of a normal gaussian distribution. (D) The occupancy distribution of the microchambers under the two conditions: 1.25 and 2.5 ng/mL *β*-gal in gray and yellow, respectively. The FDG concentration of 200 μM was the same. The bars show the ratio of the microchambers with an occupancy of *N* enzymes (*N* = 0, 1, 2, 3, 4). The triangles and the circles indicate the probability of the ratio of the microchambers-captured *N* enzymes at λ = 1.4 and 0.7, respectively, assuming the Poisson distribution. Detailed explanation is described in the main text. All the fluorescent images were captured under the illumination of 9.6 μW excitation laser.

(Figure 3(C, F)). As elucidated by the former research,[2] the increase of fluorescence intensity seemed quantized depending on the number of enclosed *β*-gal. The occupancy probability of the number of enclosed *β*-gal, *X*, can be assumed to follow Poisson distribution expressed in the following equation;[32]

$$X = \frac{\lambda^N \cdot e^{-\lambda}}{N!} \quad (2)$$

where λ is the expected number of enzymes enclosed in chamber, *N*! is the factorial of the probability mass function of *X*. As shown in Figure 3(G), λ=0.8 and 1.6 approached the observed ratio of chambers at 0.5 ng/ml and 1.0 ng/ml of *β*-gal concentration, respectively. Therefore, enclosing *β*-gal into the microchambers at a single enzyme level was confirmed. Hydrolysis rates of a single *β*-gal were calculated based on the results of Figure 3(C and F) and the standard curve of the fluorescence intensity of Fluorescein in the chambers shown in Figure S3(D). As a result, the hydrolysis rate was 16.0±1.2 s^{-1}, which is almost the same kinetics in bulk experiment, 18.0 s^{-1}. In the 61-fL microchambers, the size of reaction chamber seemed to have no effect on the enzyme reaction kinetics.

The same experiments were performed using 7.2-fL microchambers and 510-aL nanochambers, and then the hydrolysis rates were calculated. Compared to the previous experiment using 61-fL microchambers, higher concentration of *β*-gal in the assay solution was used because of an increasing number of microchambers within the same area. Figure 4 and 5 show fluorescent images, histograms, and occupancy distribution in 7.2-fL and 510-aL chambers, respectively. As analyzed previously, single enzyme hydrolysis rates were calculated as 5.7±0.96 s^{-1} and 1.9±0.27 s^{-1} in 7.2-fL and 510-aL chambers, respectively. Although the *β*-gal hydrolysis rate in 61-fL chambers was comparable to the value in bulk, the hydrolysis rate in 7.2-fL and 510-aL chambers were decreased in proportion to the size of the reaction chambers. Various factors might affect the changes, e.g. exhaustion of substrates, adsorption of *β*-gal onto the chamber surface, and photobleaching of the product. These issues were addressed by the following experiments.

According to the size reduction of the chambers, absolute number of the substrate, FDG, decreased and the observed k_{cat} might not reflect the potential maximum hydrolysis rate at saturating concentrations of FDG. To prove the all observed enzyme reactions were occurred at enough high substrate concentrations, FDG concentration was varied from 200 to 400 μM under the fixed concentration of *β*-gal at 6.25 ng/mL in 510-aL chamber and measured the single *β*-gal hydrolysis rate. As shown in the histogram in Figure S4, the peak positions at two different concentration condition were not changed. Therefore, even in the minimum reaction space in this experiment, 510 aL, the FDG concentration of 200 μM was enough high to exploit the hydrolysis rate of *β*-gal. This can be a reasonable concentration when the molar concentration translates to the number concentration of the substrate; 200 μM corresponds to 7.3×10^9, 8.6×10^8, and 6.1×10^7 FDGs in 61 fL, 7.2 fL, and 510 aL, respectively.

A major concern of a single enzyme assay is adsorption of an enzyme and a substrate onto the chamber surface. PDMS surface hydrophobicity and fast hydrophobic recovery after plasma treatments are well-known unfavorable properties especially for biological assays. Because the microchambers have larger surface area compared to conventional microtubes, the surface effect cannot be negligible for the enzyme kinetic assay. The specific surface areas of microchambers used in this experiment were 1.70 μm^{-1}, 2.93 μm^{-1}, 6.94 μm^{-1} in 61 fL, 7.2 fL,

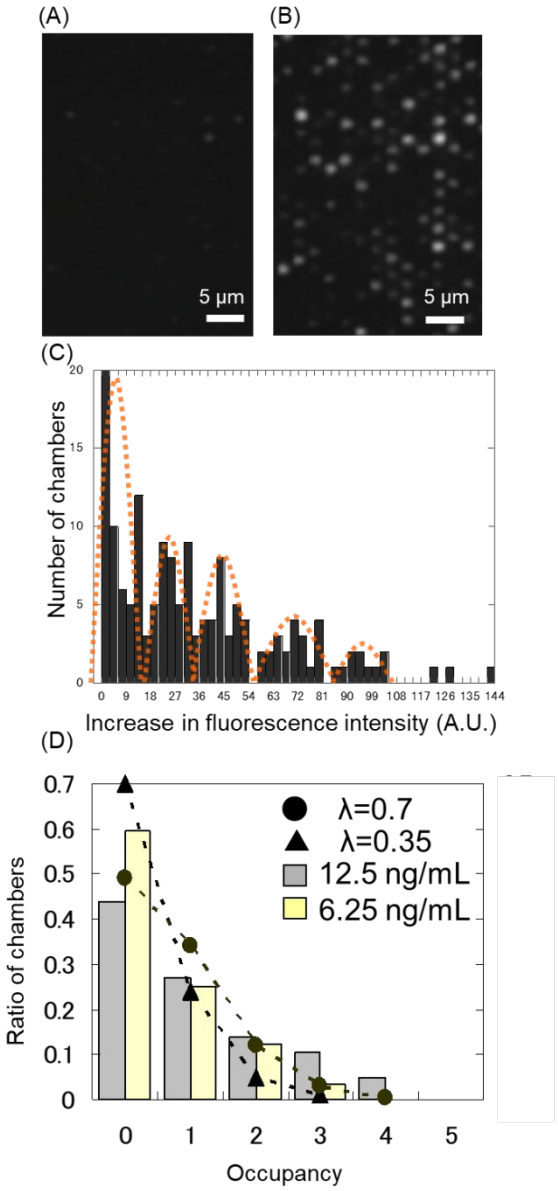

Figure 5. Single-enzyme assay in the 510-aL chambers. The fluorescent images of the microchamber array-enclosed *β*-gal after times (A) 0 and (B) 1 min. (C) Histogram of the changes in the fluorescent intensity for 2 min (n = 157). The concentrations of *β*-gal and FDG were 12.5 ng/mL and 200 μM, respectively. The five peaks in (C) are attributable to the occupancies of 0, 1, 2, 3, and 4 enzymes per chamber. The red dotted lines are guides to the eyes on the assumption of a normal Gaussian distribution. (D) Occupancy distribution of the microchambers under the two conditions: 12.5 and 6.25 ng/mL *β*-gal in gray and yellow, respectively. The concentration of FDG was the same (200 μM). The bars show the ratio of the microchambers with occupancies of *N* enzymes (*N* = 0, 1, 2, 3, 4). The triangles and circles indicate the probability of the ratio of the microchambers-captured *N* enzymes at λ = 0.35 and 0.7, respectively, following the Poisson distribution. Detailed explanation is presented in the main text. All the fluorescent images were captured under the illumination from a 3.9-μW excitation laser.

and 510 aL chambers, respectively. Considering the results of the single *β*-gal kinetic assay, the activities seems to be in inverse proportion to the reaction space. So, to evaluate adsorption of *β*-gal and FDG onto the chamber surface, push and pull of the microchamber experiments were performed as shown in Figure S5. In this experiment, the enclosed *β*-gal, FDG, and Fluorescein can be freely moved to the other microchamber after releasing the force applying to the PDMS because the partition of the microchamber is detached from the cover glass surface. Both size of microchambers showed increase and decrease of fluorescence in the different spots by repeating push and pull operation. This result strongly supports non-specific adsorption onto the surface did not affect the enzyme kinetics. Another approach to evaluate adsorption of *β*-gal and FDG onto the chamber surface was performed by SLBs coating of PC before a single enzyme assay. One mg/mL of FITC-BSA was dropped on the 7.2-fL chambers and washed with phosphate buffer for several times, and then, the microchambers were observed by TIRFM. As shown in Figure S6, although many aggregates of FITC-BSA were observed at the wall of the 7.2-fL microchambers without SLBs coating, no fluorescence signal was detected from the inside of the microchambers with SLBs coating. To verify the effect of the SLBs coating, a single enzyme assay enclosing *β*-gal was performed and the single *β*-gal hydrolysis rate was calculated as 7.8 s^{-1} which was almost the same in non-coated microchambers, 5.7±0.96 s^{-1}. Sari *et al.* addressed the adsorption issue by immobilizing *β*-gal on polystyrene beads through Schiff bases, and found about three-times increase in k_{cat} upon covalent and coordination bonding based immobilization whereas hydrogen bonding based immobilization decreased k_{cat} by 70%.[33] Considering this report, it might be reasonable that the plasma treated PDMS surface adsorbed *β*-gal through hydrogen bonding and decreased the hydrolysis rate about 70% without SLBs coating, from 7.8 to 5.7 s^{-1}. Although SLBs on PDMS surface might exert the similar effect through hydrogen bonding, the lipids in a bilayer are generally free to diffuse laterally and release the restraint of *β*-gal from the surface.

Photobleaching of the product, Fluorescein, is a crucial factor for precise quantitative evaluation of enzyme kinetics. Here 0.5 μM of Fluorescein solution was enclosed in the three different sizes of chambers and excitation light was continuously illuminated to verify the photobleaching. (In the single enzyme assay, a shutter was used to minimize the photobleaching.) As shown in Figure S7, slight photobleaching was observed during the 50-s illumination, but it was not reaction space size-dependent manner.

Enzyme kinetic assays under molecular crowding conditions

In this study, Ethylene glycol (EG), PEG-200, PEG-8,000, PEG-20,000, and BSA were used as molecular crowding agents to evaluate how the molecular crowders affect hydrolysis rate of *β*-gal. It has been reported that the quadruplex structure of DNA or RNA is stabilized in a solution of high concentration of PEG, while the double-stranded structure is destabilized,[15, 34] and

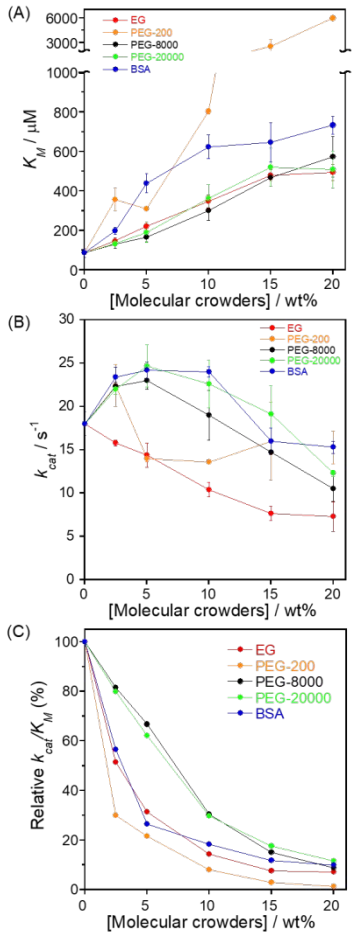

Figure 6. Kinetic parameters ((A) K_M, (B) k_{cat}, and (C) relative catalytic efficiency) as a function of the concentration of the molecular crowders. The values are the mean ± standard deviation of at least two experiments in (A) and (B). The relative catalytic efficiencies were calculated by dividing each average values of K_M and K_{cat}.

that the ribozyme kinetics is changed.[35] In addition to the influence on the structure of nucleic acids, it has also been reported that the enzymatic reaction rate changes under molecular crowding condition with high concentration of PEG molecules compared to that in dilute solution.[16, 36] The behavior of proteins especially enzyme molecules in crowded environments is mainly categorized into protein (enzyme)–molecular crowder (PEG) and protein (enzyme)–protein (BSA) interactions and their interaction manners are dominated by an entropic effect such as excluded volume and a soft chemical interaction such as hydrogen bonding, respectively.[37] Therefore, in this study, a different type of molecular crowders, PEG and BSA, was chose and investigate the influence on the enzyme kinetics.

As shown in Figures 6, the K_M increased according to the concentration of molecular crowders, especially the K_M in PEG-200 solution increased thousands of times more. The hydrolysis rate of FDG showed the maximum value at 5 to 10 wt% of BSA, PEG-8,000, and PEG-20,000 solution. On the other hand, the hydrolysis rate in PEG-200 was increased at 2.5% once and then return to the same level of bulk measurements, ~18.0 s^{-1}. The hydrolysis rate in EG was linearly decreased according to the concentration. Increase of the viscosity of the reaction solution (Fig. S8(A)) is a possible cause affecting the enzyme reaction by

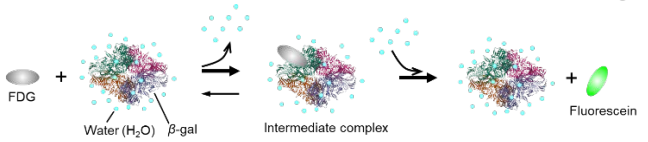

Figure 7. Scheme of the effects of the hydration and dehydration processes on the k_{cat} of FDG by β-gal.

providing diffusion-limited. In the case of PEG-8,000 and PEG-20,000, the viscosities changed significantly as the concentration increased but almost no viscosity changes were observed at any concentration of PEG-200, EG, and BSA solution. Even though the viscosity change of BSA solution is much smaller than that of PEG-8,000 and PEG-20,000 solution, the K_M and the hydrolysis rate showed a very similar trend as shown in Figure 6. This result indicates that an entanglement of PEG chain and the specific interaction with enzymes are not responsible for the change in the reaction rate constant.

The change in hydrolysis rate, k_{cat}, in a molecular crowding environment originally had been attributed to the increase in substrate concentration due to the excluded volume effect[38] and the restriction of substrate diffusion.[39] More recently, however, it has become clear that the effect of these molecular crowding agents on the enzymatic reaction is largely due to changes in the solvent environment surrounding the reaction system.[40] Unlike in diluted condition, the addition of molecular crowders in high concentration adopts the crowders themselves to be a hydrated structure, resulting in more bound water molecules and fewer free water molecules. In fact, such changes in the water surroundings have been reported to affect the polymerase kinetics of DNA.[41] The authors discussed that the effect is due to changes in the stability of the hydration structure of the unbound state of DNA, polymerase, DNA-polymerase complex, and the post-reaction state. The same might be true in the β-gal hydrolysis reaction, the number of water molecules required for the hydration in the intermediate complex of FDG and β-gal might be smaller than they exist individually and freely. When Fluorescein and two galactoses are released from the intermediate complex, more water molecules are needed than the beginning of the reaction. The reason why the hydrolysis rate increases at the lower concentration range of PEG and BSA might be because the presence of the molecular crowders stabilizes the intermediate complex, which requires fewer water molecules for hydration, thus accelerating the intermediate complex formation reaction. In contrast, the decrease in hydrolysis rate at the higher concentration range of PEG is thought to be due to the high concentration of molecular crowders, resulting in fewer free water molecules mediating the dissociation reaction of FDG and β-gal complex and the products release (Fig. 7). Unlike BSA, EG, PEG-8,000 and PEG-20,000, the K_M dramatically increased according to the concentration of PEG-200 while the hydrolysis rate did not show a specific tendency. The hydrolysis rate in EG showed linear decrease according to the concentration. These results suggest that the hydration manner of molecular crowders directly affect the hydration status of coexisting molecules. It is thought that PEG, BSA, and EG caused a decrease of the water activity and an exclusion volume effect especially in the case of PEG and BSA, which lowered the free

energy of the intermediate complex formed by β-gal and FDG, resulting in an increase of K_M. As for k_{cat}, at concentrations up to about 10 wt%, in addition to the effect of thermodynamics described above, k_{cat} is thought to have increased due to the increase in the effective concentration of β-gal (thermokinetic effect < thermodynamic effect). At higher concentrations over 10 wt%, the effect of the decrease in diffusion rate might exceed the effect of the change in free energy (thermokinetic effect > thermodynamic effect), and k_{cat} was considered to have decreased. However, since EG is a small molecule, it does not contribute to the increase in diffusion rate. Therefore, k_{cat} is considered to have decreased linearly due to the decrease in the reaction rate from the intermediate complex to the products caused by the decrease of the water activity.

Hydrolysis kinetics of β-gal in different types of confined geometries

The hydrolysis rate of a single β-gal in the microchambers decreased to 16 ± 1.2, 5.7 ± 0.96, and 1.9 ± 0.27 s^{-1} as the reaction volume decreased from 61 fL, 7.2 fL, and 510 aL, respectively. In contrast, a molecular crowder, PEG-8,000, increased the hydrolysis rate once and then decreased according to the concentration as shown in Figure 6(B). To discuss the substantial difference of the hydrolysis rate in both experimental systems, we focused on molecular diffusion in each system by measuring mean square displacements (MSDs) of a 50-nm diameter fluorescent particle in each system and investigate how the limited diffusion affect the hydrolysis rate. As shown in Figure S9, the trajectories of the fluorescent particles were traced every 33 ms as flat two-dimensional motion and the MSDs, $<R^2>$, was calculated by the following equation.

$$< R^2 >= \frac{1}{N}\sum_{i=1}^{N}[\Delta Ri(t)]^2 \quad (3)$$

$$[\Delta Ri(t)]^2 = [\Delta xi(t)]^2 + [\Delta yi(t)]^2 \quad (4)$$

where N is the number of trajectory plots of fluorescent beads, and $[\Delta Ri(t)]^2$ is the square displacement from time t to t+33 ms. The MSDs in the chambers converged to the constant values over time and these values were closest to the MSDs in solution containing PEG-8,000. As shown in Figure 8(A), MSDs in 5.0 wt%, 10 wt%, and 20 wt% of PEG-8,000 solution showed similar values in 61 fL, 7.2 fL, and 510 aL chambers, respectively. In terms of the diffusion manner, the smallest chamber, 510 aL, offered almost the same diffusion limited system of PEG-8,000 solution at 20 wt% and enabled to mimic the molecular crowding condition like inside of bacteria and cell nucleus which have typically about 2 fL and 70 fL volume, respectively. However, as shown in Figure 8(B), the hydrolysis rate of a single β-gal in the microchamber was lower than that in the solution filled with molecular crowders, probably due to some kind of influence from the PDMS surface such as hydrophobic effect through the substrates, FDG, and long-range interaction through structured water molecules.[42] Although thermodynamic parameter, K_M, could not estimate from the classical Michaelis-Menten equation in the microchambers system, the large hydrophobic surface area might cause increase water activity and excluded volume effect which

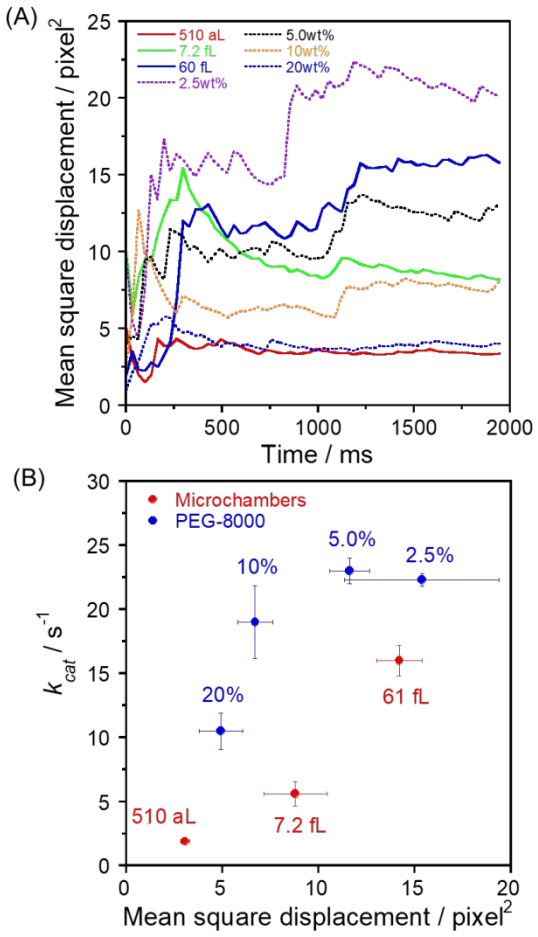

Figure 8. (A) MSDs of a 50-nm diameter fluorescent particle as a function of time in the microchambers and in the solution containing PEG-8,000 at different concentration. (B) k_{cat} of β-gal as a function of MSDs in the microchambers and under the molecular crowding condition. The error bars of MSDs were calculated from 2-s observation.

directly affect the structure of β-gal and its intermediate complex. Therefore, the different tendency of k_{cat} values as a function of MSD in the microchambers and the molecular crowder systems might attribute to misplace of thermodynamic effect in the microchambers system. Experimental platforms for thermodynamic analysis at a single enzyme level are eagerly anticipated to address the issue.

Conclusions

Several factors potentially affecting the enzyme kinetics such as adsorption and substrate loss were carefully studied and optimized the chamber platform for a single enzyme kinetics study. Hydrolysis rates of β-gal enclosed in the chambers at a single enzyme level was measured, and as a result, the rates were decreased to 16±1.2, 5.7±0.96, and 1.9±0.27 s^{-1} according to the decrease of the reaction volume from 61 fL, 7.2 fL, and 510 aL, respectively. Based on the molecular diffusion manners of MSDs in the confined space and the molecular crowding conditions, the single enzyme kinetics was studied and found that the kinetics could not simply understand from diffusion-limited space corresponding to the reaction frequency of the substrate and the enzyme. Although thermodynamic

parameters on a single enzyme reaction in the chamber system could not obtain, evaluation methods of a substrate and an enzyme affinity including energetic state of the intermediate complex are expected as well as experimental platform, e.g. PEG-modified chambers, vesicles and emulsions array, toward understanding the enzyme reaction *in vivo* environments.

Author Contributions

All the authors have approved the final version of the manuscript.

Conflicts of interest

There are no conflicts to declare.

Acknowledgements

This work was partially supported by JST/PRESTO (Grant number JPMJPR16F4); JSPS KAKENHI (Grant Numbers JP21H01966, JP20H04714, and JP19KK0140); and research grants from the Shimadzu Science Foundation, Toyota Riken Scholar, and the Casio Science Promotion Foundation.

Notes and references

1. L. Michaelis and M. L. Menten, *Biochem Z*, 1913, **49**, 333-369.
2. Y. Rondelez, G. Tresset, K. V. Tabata, H. Arata, H. Fujita, S. Takeuchi and H. Noji, *Nat Biotechnol*, 2005, **23**, 361-365.
3. D. M. Rissin and D. R. Walt, *J Am Chem Soc*, 2006, **128**, 6286-6287.
4. D. M. Rissin and D. R. Walt, *Nano Lett*, 2006, **6**, 520-523.
5. R. Watanabe, N. Soga, D. Fujita, K. V. Tabata, L. Yamauchi, S. Hyeon Kim, D. Asanuma, M. Kamiya, Y. Urano, H. Suga and H. Noji, *Nat Commun*, 2014, **5**, 4519.
6. R. Watanabe, T. Komatsu, S. Sakamoto, Y. Urano and H. Noji, *Lab Chip*, 2018, **18**, 2849-2853.
7. S. Sakamoto, T. Komatsu, R. Watanabe, Y. Zhang, T. Inoue, M. Kawaguchi, H. Nakagawa, T. Ueno, T. Okusaka, K. Honda, H. Noji and Y. Urano, *Sci Adv*, 2020, **6**, eaay0888.
8. N. Soga, R. Watanabe and H. Noji, *Sci Rep*, 2015, **5**, 11025.
9. Y. Zhang, Y. Minagawa, H. Kizoe, K. Miyazaki, R. Iino, H. Ueno, K. V. Tabata, Y. Shimane and H. Noji, *Sci Adv*, 2019, **5**, eaav8185.
10. K. V. Tabata, Y. Minagawa, Y. Kawaguchi, M. Ono, Y. Moriizumi, S. Yamayoshi, Y. Fujioka, Y. Ohba, Y. Kawaoka and H. Noji, *Sci Rep*, 2019, **9**, 1067.
11. Y. Minagawa, H. Ueno, K. V. Tabata and H. Noji, *Lab Chip*, 2019, **19**, 2678-2687.
12. H. H. Gorris, D. M. Rissin and D. R. Walt, *Proc Natl Acad Sci U S A*, 2007, **104**, 17680-17685.
13. Y. Jiang, X. Li, B. R. Morrow, A. Pothukuchy, J. Gollihar, R. Novak, C. B. Reilly, A. D. Ellington and D. R. Walt, *ACS Cent Sci*, 2019, **5**, 1691-1698.
14. D. S. Goodsell, *Trends Biochem Sci*, 1991, **16**, 203-206.
15. S. Matsumoto, H. Tateishi-Karimata, S. Takahashi, T. Ohyama and N. Sugimoto, *Biochemistry*, 2020, **59**, 2640-2649.
16. X. E. Wilcox, A. Ariola, J. R. Jackson and K. M. Slade, *Biochemistry*, 2020, **59**, 1737-1746.
17. K. Kohata and D. Miyoshi, *Biophys Rev*, 2020, **12**, 669-676.
18. J. Hofmann and M. Sernetz, *Analytical Biochemistry*, 1983, **131**, 180-186.
19. Z. J. Huang, *Biochemistry*, 1991, **30**, 8535-8540.
20. Z. J. Huang, *Biochemistry*, 1991, **30**, 8530-8534.
21. E. F. Tsung and R. D. Tilton, *J Colloid Interface Sci*, 1999, **213**, 208-217.
22. C. W. Brown Iii, E. Oh, D. A. Hastman, S. A. Walper, K. Susumu, M. H. Stewart, J. R. Deschamps and I. L. Medintz, *RSC Advances*, 2015, **5**, 93089-93094.
23. A. P. Malanoski, J. C. Breger, C. W. Brown, J. R. Deschamps, K. Susumu, E. Oh, G. P. Anderson, S. A. Walper and I. L. Medintz, *Nanoscale Horiz*, 2017, **2**, 241-252.
24. J. C. McDonald, D. C. Duffy, J. R. Anderson, D. T. Chiu, H. Wu, O. J. Schueller and G. M. Whitesides, *Electrophoresis*, 2000, **21**, 27-40.
25. T. Yang, S. Jung, H. Mao and P. S. Cremer, *Anal Chem*, 2001, **73**, 165-169.
26. J. A. Jackman and N. Cho, *Langmuir*, 2020, **36**, 1387-1400.
27. B. J. Burke and F. E. Regnier, *Electrophoresis*, 2001, **22**, 3744-3751.
28. M. Abel, A. Planas and U. Christensen, *Biochem. J.*, 2001, **357**, 195-202.
29. N. Cruys-Bagger, J. Elmerdahl, E. Praestagaard, H. Tatsumi, N. Spodsberg, K. Borch and P. Westh, 2012, **287**, 18451-18458.
30. J. Monahan, A. A. Gewirth and R. G. Nuzzo, *Anal Chem*, 2001, **73**, 3193-3197.
31. K. Hosokawa, K. Sato, N. Ichikawa and M. Maeda, *Lab Chip*, 2004, **4**, 181-185.
32. H. C. Arai, A. Yukawa, R. J. Iwatate, M. Kamiya, R. Watanabe, Y. Urano and H. Noji, *Biophys J*, 2014, **107**, 156-164.
33. E. Aynaci, N. Sari and H. Tumturk, *Artif Cells Blood Substit Immobil Biotechnol*, 2011, **39**, 259-266.
34. D. Miyoshi and N. Sugimoto, *Biochimie*, 2008, **90**, 1040-1051.
35. S. DasGupta, *Org Biomol Chem*, 2020, **18**, 7724-7739.
36. A. E. Wilcox, M. A. LoConte and K. M. Slade, *Biochemistry*, 2016, **55**, 3550-3558.
37. C. Ota and K. Takano, *Langmuir*, 2016, **32**, 7372-7382.
38. A. P. Minton, *Mol Cell Biochem*, 1983, **55**, 119-140.
39. R. J. Ellis, *Curr Opin Struct Biol*, 2001, **11**, 114-119.
40. S. Nakano, H. Karimata, T. Ohmichi, J. Kawakami and N. Sugimoto, *J Am Chem Soc*, 2004, **126**, 14330-14331.
41. Y. Sasaki, D. Miyoshi and N. Sugimoto, *Biotechnol J*, 2006, **1**, 440-446.
42. T. Tsukahara, A. Hibara, Y. Ikeda and T. Kitamori, *Angew Chem Int Ed Engl*, 2007, **46**, 1180-1183.